Medical applications of diamond particles & surfaces

Diamond has been considered for use in several medical applications due to its unique mechanical, chemical, optical, and biological properties. In this paper, methods for preparing synthetic diamond surfaces and particles are described. In addition, recent developments involving the use of diamond in prostheses, sensing, imaging, and drug delivery applications are reviewed. These developments suggest that diamond-containing structures will provide significant improvements in the diagnosis and treatment of medical conditions over the coming years.

Roger J Narayan[a], Ryan D. Boehm[a], and Anirudha V. Sumant[b]

[a]Joint Department of Biomedical Engineering, University of North Carolina and North Carolina State University, Raleigh, NC, USA

[b]Center for Nanoscale Materials, Argonne National Laboratory, Argonne, IL, USA

**E-mail: roger_narayan@unc.edu*

Diamond is an allotrope of carbon that is being considered for use in several medical applications[1]. Ramachandran determined that the crystal structure of diamond consists of two close packed interpenetrating face centered cubic lattices; one lattice is shifted with respect to the other along the elemental cube space diagonal by one-quarter of its length[2]. If one approximates carbon atoms as equal diameter rigid spheres, the filling of this construction is 34 %[3]. Due to the carbon-carbon distance (1.54 Å), diamond crystal exhibits the highest atomic density (1.76×10^{23} cm^{-3}) of any solid. The very high bond energy between two carbon atoms (83 kcal/mol) and the directionality of tetrahedral bonds are the main reasons for the high strength of diamond. Diamond demonstrates the highest Vickers hardness value of any material (10 000 kg/mm^2). The tribological properties of diamond are also impressive; the coefficient of friction of polished diamond is 0.07 in argon and 0.05 in humid air. Diamond is resistant to corrosion except in an oxygen atmosphere at temperatures over 800 °C. In addition, type IIa diamond exhibits the highest thermal conductivity of all materials (20 W cm^{-1} K^{-1} at room temperature).

Growth of synthetic diamond

The graphite-diamond transformation at thermodynamic equilibrium necessitates the use of very high temperatures and pressures. Bundy *et al.* at General Electric developed a high pressure-high temperature approach for creating diamond from graphite in the 1950s[4]. This technique creates small diamond crystals that are commonly utilized for polishing, cutting, and grinding. Growth of diamond coatings at low pressure using hydrocarbon pyrolysis was first reported by Eversole *et al.* at Union Carbide in 1962[5]. In the late 1960s and early 1970s, Derjaguin *et al.* and Angus *et al.* introduced the concept of activating a mixture containing hydrogen and a hydrocarbon gas for low-pressure chemical vapor deposition of diamond coatings[6,7]. For example, Angus *et al.* demonstrated deposition of diamond layers on natural diamond powder by thermal decomposition of methane at a temperature of 1050 °C and a pressure of 0.3 Torr[7]. In these methods, diamond coatings are grown

ISSN:1369 7021

from an activated gas phase; this phase contains hydrogen (~99 %) as well as methane or other carbon-containing gases. Activation of the gas commonly involves the use of a hot filament, combustion flame, plasma, or a combination of these approaches. Diamond coatings are formed by the decomposition of activated hydrocarbon species into excited carbon atoms. Diamond coatings are commonly deposited on metallic substrates for minimizing wear, corrosion, and metal release; for example, a diamond-coated metallic implant will behave mechanically as the metallic substrate and chemically as the diamond coating.

Several parameters must be considered in deposition of microcrystalline diamond coatings. Hydrogen serves several roles, including termination of carbon dangling bonds, stabilization of diamond clusters, removal of sp^2-hybridized carbon from the surface, and abstraction of hydrogen from carbon-hydrogen bonds on the surface[8]. The chemical properties of the substrate regulate the structure of the diamond coating[9]. Diamond coating growth on cobalt, ferrous alloys, and nickel alloys is challenging because the nucleation of diamond is hindered by high carbon diffusion rates within these materials[10]. Formation of graphite is commonly observed on nickel and other elements that contain partially-filled electron shells.

Growth of microcrystalline diamond on non-diamond surfaces involves scratching of the substrate to promote diamond nucleation and/or use of an interlayer between the diamond coating and the non-diamond substrate. Ultrasonic seeding of the substrate with ultradispersed detonation diamond has also been used to increase the nucleation of diamond[11,12]. It should be noted that scratching may alter the surface in a poorly-defined manner; non-uniform features may limit use of the coated material in medical applications. In addition, heterogeneous films containing diamond and graphitic carbon may be created on substrates that are scratched with diamond paste[10].

An interlayer material (e.g., titanium nitride, aluminum nitride, and tungsten carbide) can promote diamond nucleation and facilitate coating adhesion through relief of interfacial stresses[13]. Properties of the interlayer material include: a similar thermal expansion coefficient value to that of diamond for reducing thermal stresses; low diffusivity of carbon for increasing diamond nucleation; and small lattice mismatch with diamond as well as with the bulk material. Silicon nitride is frequently utilized as a bulk material due to the fact that it exhibits a low coefficient of thermal expansion. In addition, silicon nitride exhibits high fracture toughness and high hardness values[14,15]. Furthermore, silicon nitride is compatible with diamond CVD deposition temperatures (650 – 1000 °C).

Significant academic and industrial research activities are underway to create nanocrystalline diamond coatings. The term nanocrystalline diamond is utilized for describing materials that contain grain sizes below 100 nm, usually 10 – 100 nm (Fig. 1)[16]. The mechanism for nanocrystalline diamond growth, which involves a hydrogen-rich growth chemistry, is similar to that for microcrystalline diamond or polycrystalline diamond growth. Competitive crystal growth results in a columnar texture that is oriented in the growth direction and the

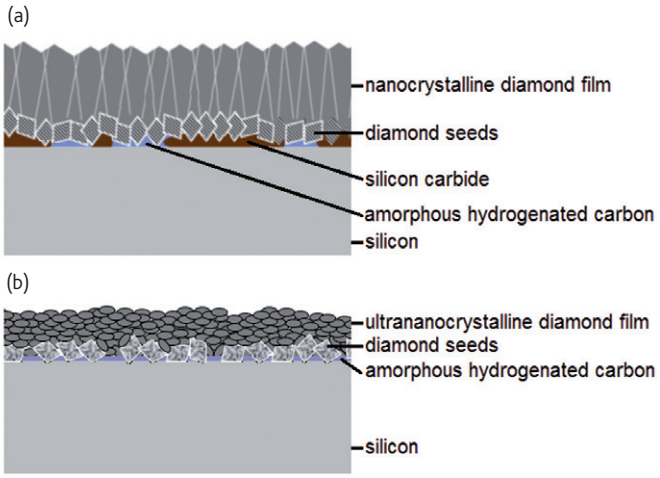

Fig. 1 Schematic explaining the possible nucleation mechanisms of (a) nanocrystalline diamond and (b) ultrananocrystalline diamond. Reproduced with permission from[16]. © Wiley-VCH Verlag GmbH & Co. KGaA.

coarsening of grain sizes with film thickness (van der Drift growth). By controlling the initial nucleation density and the growth parameters, one can limit re-nucleation density and maintain grain sizes from 10 to 100 nm for nanocrystalline diamond films up to a few micrometers in thickness. When film thickness exceeds a few micrometers, nanocrystalline diamond growth behaves like microcrystalline diamond growth; in this situation, roughness increases with film thickness.

Nanocrystalline diamond coatings exhibit small crystallite sizes; these materials are considered to be appropriate for tribological applications due to their relatively smooth surfaces. Amaral *et al.* examined the wear behavior of nanocrystalline diamond; steady-state friction coefficients of 0.01 – 0.05 in unlubricated environments and water-lubricated environments were observed[17]. The wear rate under water lubrication was 1.9 x 10^{-10} mm^3 N^{-1} m^{-1}; testing in Hank's balanced salt solution revealed similar friction (0.06) and wear data. Testing in dilute fetal bovine serum revealed a higher coefficient of friction (0.10); this finding was associated with protein attachment. Wear behavior in Ringer's solution and synthetic serum was impressive; final wear rates of ~10^{-10} mm^3 N^{-1} m^{-1} were obtained.

The term ultrananocrystalline diamond was coined by researchers at Argonne National Laboratory to distinguish their form of diamond from other forms of diamond on the basis of grain size. Ultrananocrystalline diamond contains grains with sizes below 10 nm, usually between 2 and 5 nm. 95 – 98 % of the material, in the form of sp^3-hybridized carbon, is found in these grains; the remaining material, in the form of sp^2-hybridized carbon, resides at atomically abrupt grain boundaries[18,19]. Ultrananocrystalline diamond films are produced in an argon-rich, hydrogen-deficient environment using microwave plasma-enhanced chemical vapor deposition. Films grown from plasmas containing ~99 % argon and ~1 % methane are able to grow directly on SiO_2 since carbon dimers (C_2) form a silicon carbide nucleation layer. Work by Sumant *et al.* and Naguib *et al.* has indicated that a tungsten

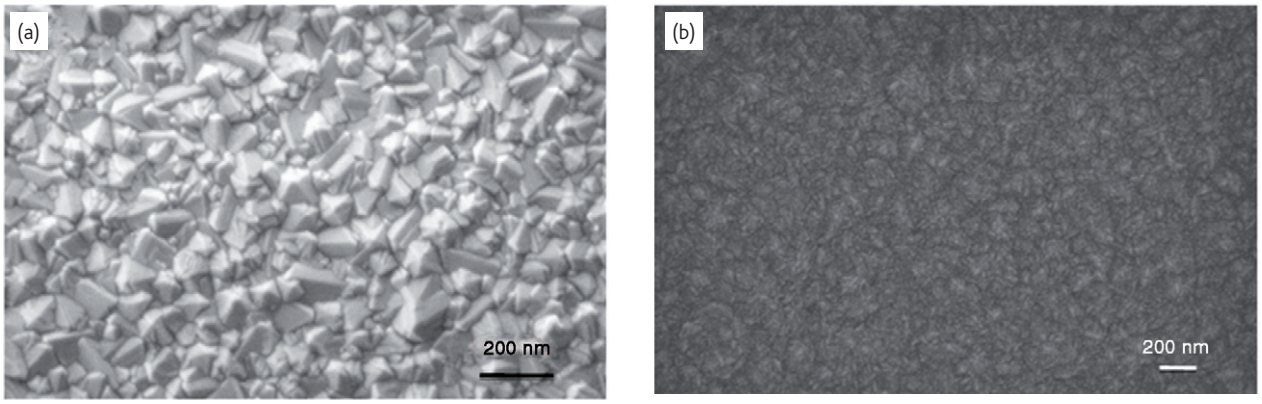

Fig. 2 Scanning electron micrograph images depicting typical surface morphologies of (a) nanocrystalline diamond and (b) ultrananocrystalline diamond films. Reprinted from[23,24] with permission.

interlayer reduces the incubation time for diamond nucleation due to the low diffusion coefficient of carbon in tungsten; as a result, ultrananocrystalline diamond coatings may be grown with lower surface roughness values (4 – 6 nm), lower thickness values, and an absence of interfacial voids[20,21]. High re-nucleation (~10^{11} cm^{-2} s^{-1}) and minimal re-gasification of small grains occur due to a limited amount of hydrogen in the plasma[18,19]. In addition, ultrananocrystalline diamond can be deposited at temperatures as low as 400 °C, facilitating use of this material in complementary metal-oxide-semiconductor (CMOS)-compatible microelectromechanical systems (MEMS) or nanoelectromechanical systems (NEMS)[22].

The exceptional chemical and physical properties of nanocrystalline diamond and ultrananocrystalline diamond determine the medical applications of these materials[18,19]. Figs. 2a and b show scanning electron microscopy images that depict typical surface morphologies of nanocrystalline diamond and ultrananocrystalline diamond films, respectively[22,23]. There is a distinct difference in surface morphologies of nanocrystalline diamond and ultrananocrystalline diamond films. Nanocrystalline diamond shows some grain faceting along with some secondary nucleation. On the other hand, no grain faceting can be seen in ultrananocrystalline diamond; this morphology is attributed to a very high re-nucleation rate during film growth.

Fig. 3a contains a selected area electron diffraction pattern for a nanocrystalline diamond coating on a silicon (100) substrate; (111), (022), (113), (222), (004), and (133) reflections of cubic diamond were observed[24]. The bright ring was assigned to diamond-like carbon and/or amorphous glassy carbon within the coating. No significant scattering attributable to graphite crystallites was noted. Grain boundaries of ~1 nm and 2 – 4 nm rectangular crystallites were noted in the transmission electron micrograph (Fig. 3b).

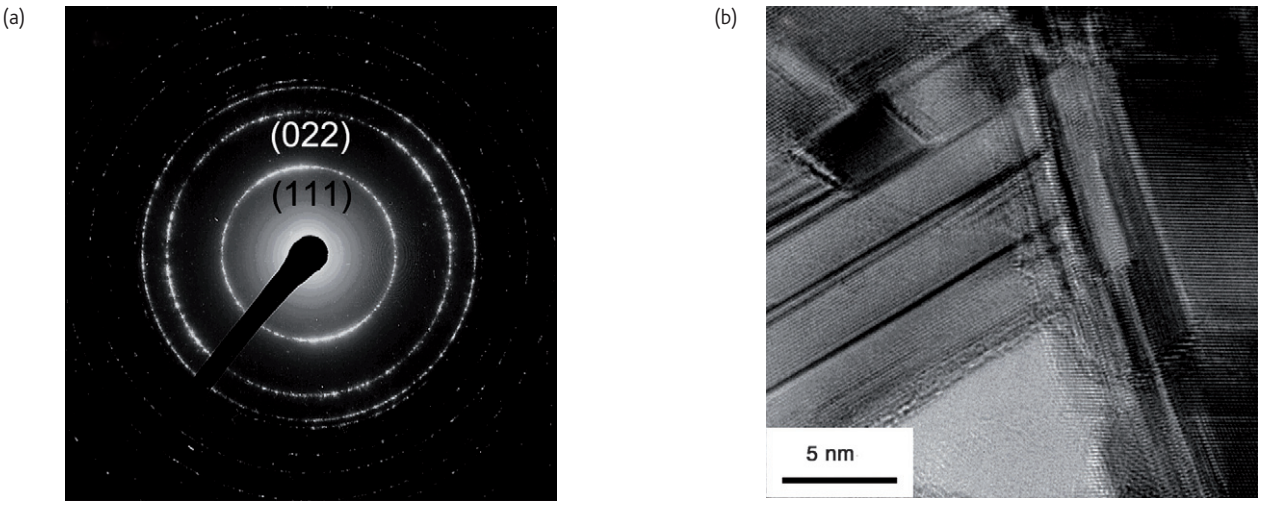

Fig. 3 (a) Selected area electron diffraction pattern of the nanocrystalline diamond coating. In this image, sharp Bragg reflections from the first two planes are indicated. The rings were indexed as (111), (022), (113), (222), (004), and (133) from the diamond cubic structure. The bright ring around the center represents the amorphous glassy carbon or diamond-like carbon material. (b) High-resolution transmission electron micrograph of the nanocrystalline diamond coating. Rectangular crystallites were observed (with a size of 2 – 4 nm). Reprinted from[25] with permission from Elsevier.

Nanodiamond particles may be produced using a variety of methods. Detonation nanodiamond was originally produced in the Soviet Union[25]. Nanodiamond particles are commonly prepared by detonating carbon-containing explosives under a rapid cooling rate (≥ 3000 K/min); the resulting polyhedral structures exhibit a narrow particle size distribution and a small particle size (3.5 – 6 nm)[26,27]. A cooling gas (e.g., carbon dioxide or an inert gas) is used to prevent the formation of graphite and other non-diamond materials[28]. After synthesis, removal of non-diamond non-carbon impurities by means of acid washing, ball milling, and/or batch ultrasonication is performed[29]. For example, Adadurov *et al.* described the preparation of nanodiamond particles using either an x-ray-amorphous form of carbon (e.g., carbon black) or graphite; explosives (e.g., PETN and hexogen) were used to create temperatures of 2000 – 6000 °C and dynamic pressures of 3 – 60 GPa[25]. Fig. 4 shows transmission electron micrographs of nanodiamond aggregates, including (a) pristine raw soot, (b) pristine soot after washing with hot nitric acid, and (c) a commercially available product. Krueger *et al.* described the use of stirred-media milling with ceramic beads (with a diameter of 0.1 mm) in order to obtain 4 – 5 nanodiamond particles[27]. High temperature-high pressure growth combined with ball milling may also be used to prepare ≥ 4 nm nanodiamond particles[30].

(a)

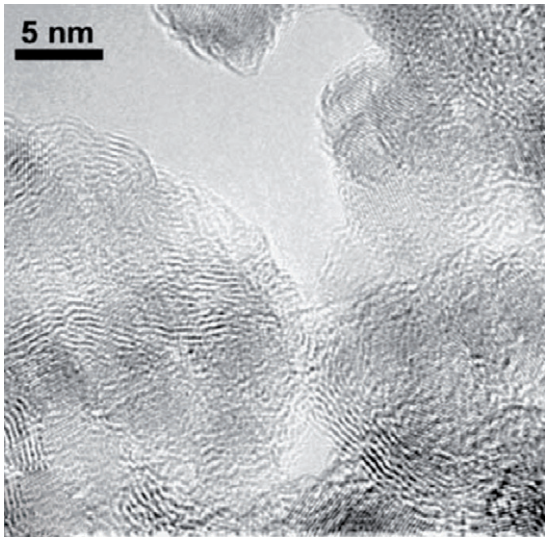

(b)

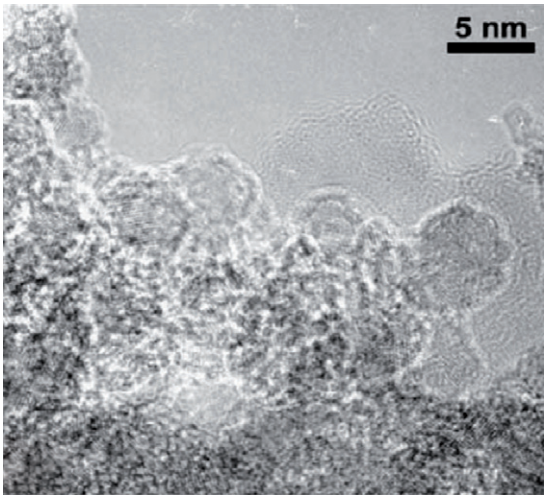

Fig. 4 Transmission electron microscopy photographs (200 keV) of nanodiamond aggregate (NDA): (a) pristine material (sample N2 in the source manuscript) (soot), (b) pristine material (N4 in the source manuscript) after washing with hot nitric acid, (c) a recent commercial product (B' in the source manuscript). Reprinted from[28] with permission from Elsevier.

Diamond-based medical devices

Diamond coatings have been applied to a number of medical devices in recent years, including temporomandibular joint prostheses, heart valves, and microelectromechanical systems, for the purpose of extending implant lifetime. Fries *et al.* performed microwave plasma chemical vapor deposition of 3 μm-thick nanostructured diamond films on objects that were similar in shape to components of temporomandibular joint prostheses[31]. Raman spectroscopy was used to demonstrate the uniform chemical composition of the nanostructured diamond coating on the surface of the titanium-aluminum-vanadium alloy condyle component. Nanoindentation hardness measurements showed that coating hardness was 60 ± 5 GPa. Papo *et al.* deposited single layer nanocrystalline diamond films and multilayer nanocrystalline/microcrystalline/nanocrystalline diamond films on Ti-6Al-4V components, which were similar in shape to the fossa and condyle components of a temporomandibular joint prosthesis[32]. Wear testing in a mandibular movement simulator corresponding to two years of clinical use was performed; micro-Raman scans of the wear-tested components revealed no film loss and some film damage. The multilayer nanocrystalline/microcrystalline/nanocrystalline diamond film showed better wear resistance than the single layer nanocrystalline diamond film.

Jozwik *et al.* deposited nanocrystalline diamond on an artificial heart valve ring using plasma-assisted chemical vapor deposition[33]. Good coverage of the nanocrystalline diamond coating on the surface of the titanium ring was noted. Raman spectroscopy and scanning electron microscopy of the nanocrystalline diamond-coated ring after mechanical fatigue testing indicated that the coating was in good condition. The nanocrystalline diamond coating remained on the entire surface after fatigue testing. Amaral *et al.* deposited nanocrystalline diamond coatings on Si_3N_4–bioglass substrates using hot filament chemical vapor deposition[34]. Pin-on-flat wear studies in Hanks' balanced salt solution and dilute fetal bovine serum provided coefficient of friction values of 0.01 – 0.02 and 0.06 – 0.09, respectively; the higher wear rate obtained with fetal bovine serum was attributed to attachment of proteins. Wear rates in Hanks' balanced salt solution and dilute fetal bovine serum were $k \sim 10^{-10}$ mm^3 N^{-1} m^{-1} and $k \sim 10^{-9} – 10^{-8}$ mm^3 N^{-1} m^{-1}, respectively.

Pecheva *et al.* described processing of a composite material containing apatite and 4 – 6 nm nanodiamond on AISI 316L stainless steel by means of potentiostatic deposition; this coating exhibited no residual stress or cracks[35]. The composite coating exhibited better adhesion, ductility, and Vickers hardness than pure apatite. The apatite-nanodiamond coating also demonstrated biological activity; formation of a hydroxyapatite layer in simulated body fluid was observed. This material may be used to prevent release of metal ions, inhibit fibrous tissue growth, and prevent blood coagulation in medical devices. Huang *et al.* created single-layer and multilayer nanofilms containing 2 – 8 nm nanodiamond particles by means of a layer-by-layer deposition approach[36]. *In vitro* studies involving RAW 264.7 murine macrophages showed that the dexamethasone-nanodiamond composite nanofilms attenuated inflammatory cytokine levels. Use of these materials as anti-inflammatory implant coatings and drug delivery devices has been considered[29,36].

Diamond may find use in microscale devices for sensing and/or drug delivery, which are known as biomedical microelectromechanical systems (bioMEMS). Conventional microelectromechanical systems are commonly fabricated using silicon; however, silicon demonstrates undesirable mechanical and tribological properties, including poor brittle fracture strength and a tendency to adhere to surfaces (stiction). Sumant *et al.* and Carpick *et al.* utilized atomic force microscopy to examine the nanoscale adhesion and friction behavior of ultrananocrystalline diamond surfaces; Sumant *et al.* showed that hydrogen-terminated ultrananocrystalline diamond exhibited a work of adhesion value of 10.2 ± 0.4 mJ/m^2, which is lower than work of adhesion values associated with saturated hydrocarbon interfaces[23,37]. This work of adhesion value was entirely attributed to van der Waals forces. Tribological studies involving self-mated ultrananocrystalline diamond surfaces have demonstrated friction coefficients as low as $\mu < 0.007$ under test conditions with sufficient humidity[38]. It should also be noted that ultrananocrystalline diamond exhibits hardness and Young's modulus values of ~98 GPa and ~980 GPa, respectively. Several methods for preparing diamond-based microelectromechanical systems, including conformal coating, selective deposition, and lithographic patterning, have been described[39,40]. Diamond film can be deposited as a thin, conformal coating using chemical vapor deposition. For example, high aspect ratio and low aspect ratio silicon tips were coated with ultrananocrytalline diamond films[39]. The selective deposition process involves growth of ultrananocrystalline diamond on only part of the substrate. Growth of ultrananocrystalline diamond requires a nucleation layer; in selective deposition, a portion of the substrate is seeded. It should be noted that the feature resolution obtained using this method is limited by the grain size. Fig. 5 shows freestanding 1 μm-thick diamond propellers, which are supported by 100 μm tall silicon platforms[39]. The long arms in these structures are flat, which indicates that that the ultrananocrystalline diamond films are nearly stress-free. Lithographic patterning may also be used to prepare multilayer structures; in this method, a thin diamond film is deposited on a sacrificial release layer (e.g., SiO_2). For example,

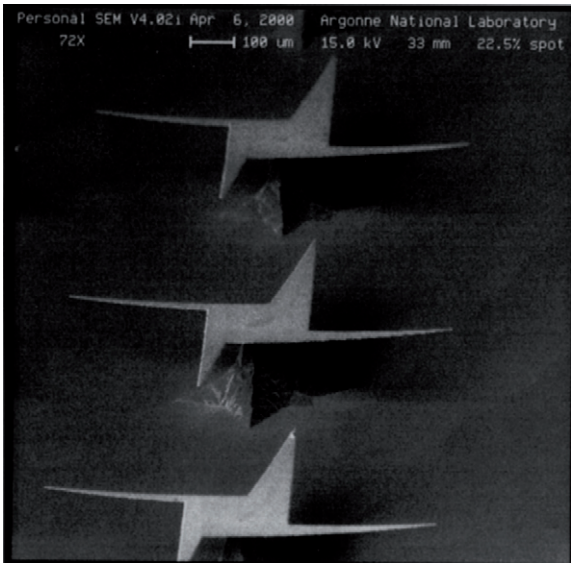

Fig. 5 Scanning electron micrograph of freestanding ultrananocrystalline diamond propellors, which were grown by selective deposition followed by potassium hydroxide etching on silicon posts. Reprinted from[40] with permission from Elsevier.

lithographic patterning of a diamond-based microelectromechanical system may involve the following steps: deposition of an ultrananocrystalline diamond coating on a thermal SiO_2 layer, deposition of a SiO_2 layer, patterning of SiO_2 with a photoresist using reactive ion etching, etching of ultrananocrystalline diamond using oxygen plasma, and removal of SiO_2 using a hydrofluoric acid wet etch and/or a gas etch. Krauss *et al.* demonstrated processing of multilevel structures, including a captive rotor, using a combination of selective deposition and lithographic etching[39].

Khanna *et al.* developed lab-on-a-chip structures containing hydrogen-terminated nanocrystalline diamond[41]. In their work, nanocrystalline diamond exhibited the least binding of DNA. In addition, nanocrystalline diamond was shown to exhibit less non-specific attachment than glass, polydimethylsiloxane, polymethylmethacrylate, silicon dioxide, silicon, or SU-8. These results suggest that nanocrystalline diamond may be used to provide high sensitivity and high throughput in lab-on-chip devices. In subsequent work, Khanna *et al.* created microspikes using nanocrystalline diamond[42]. They incorporated the spikes in a microfluidic chamber, which may be placed within a lab-on-chip system. The microspikes increased the mechanical lysis efficiency for B16-F10 (ATCC CRL-6475) murine melanoma cells as compared with non-textured glass. An increase in fluorescence of ~400 % was observed. It is interesting to note that performance of the microspikes did not diminish after multiple ultrasonic vibration/wash cycles.

Bijnens *et al.* developed an immunosensor containing nanocrystalline diamond; in this sensor, anti-C reactive protein antibodies were physically adsorbed to the surface of hydrogen-terminated nanocrystalline diamond[43]. Real-time monitoring of

C-reactive proteins was demonstrated; for example, 1 μM C-reactive protein was detected with a thirty minute reaction time. Diamond nanowire-based nucleic acid sensors have recently been developed. Nebel *et al.* described fabrication of diamond nanowires through use of an electrochemical phenyl-linker molecule attachment and functionalized thiol-modified DNA[44]. Sensitivity to hybridization of complementary DNA sequences with a concentration of 2 pM over a 3 mm^2 sensor area was demonstrated. No degradation in DNA bonding was noted over thirty hybridization/denaturation cycles.

Diamond is also an attractive material for use in cell-based biosensors. Ariano *et al.* demonstrated adhesion, growth and viability of GT1-7 neuronal cells (neuronal line of hypothalamic origin) on diamond surfaces[45]. Cells plated on H^- or O^- terminated nanocrystalline diamond samples were shown to adhere, proliferate and exhibit somatic Ca^{2+} activity. Their work suggested that hydrogen-terminated nanocrystalline diamond is a transparent, biocompatible and conductive material for cell-based biosensors. Due to its optical transparency, stable electrical conductivity, and mechanical robustness, Ariano *et al.* examined the use of diamond in the fabrication of multielectrode arrays[46]. They demonstrated fabrication of electrodes out of conductive H-terminated diamond for recording electrical signals from excitable cells. Multiparametrical recordings of electrical activity from cultured neuronal networks were demonstrated.

In addition, diamond is being considered for use in neural prostheses. Arrays of solution-gate field-effect transistors were fabricated by Dankerl *et al.* using hydrogen-terminated single-crystalline diamond substrates[47]. Adhesion of cardiomyocyte-like (HL-1) and human embryonic kidney (HEK293) cells was demonstrated. In addition, potassium currents of HEK293 cells were activated with the patch-clamp technique and observed with field-effect transistors. Furthermore, stability of the device in phosphate buffered saline electrolyte solutions for at least seven days was noted.

Xiao *et al.* discussed the development of retinal prostheses in which ultrananocrystalline diamond served as an inert coating[48]. Electrochemical inactivity and very low leakage currents were demonstrated using cyclic voltammetry. Ultrananocrystalline diamond implanted in the rabbit eyes was not associated with intraocular inflammation; however, acute tissue reactions and silicon degradation were observed with incomplete ultrananocrystalline diamond coatings. Their work suggested that intact nanocrystalline diamond coatings are appropriate hermetic coatings for retinal implants. Bonnauron *et al.* utilized detonation nanodiamond seeding and bias enhanced nucleation in order to create diamond-containing microelectrode arrays on three-dimensional glass substrates; such devices may find use in retinal implants[49].

Rezek *et al.* recently evaluated the effects of cell growth and protein adsorption on solution-gated field-effect transistors containing hydrogen-terminated nanocrystalline diamond films[50]. Interaction with fetal bovine serum proteins was shown to decrease diamond conductivity; this result was attributed to formation of a 2 – 4 nm thick protein film on the diamond surface. Incubation of osteoblastic SAOS-2 cells on the diamond field-effect transistor surface was also associated with a decrease in conductivity. It is thought that proteins lower the diamond-electrolyte electronic barrier, enabling alternate mechanisms for the transfer of charge across the diamond-electrolyte interface.

Functionalization of nanodiamond and nanocrystalline diamond

The functionalization of nanodiamond with biological molecules has attracted significant research activity in recent years. In 2002, Yang *et al.* demonstrated covalent attachment of DNA oligonucleotides to nanocrystalline diamond[51]. In the initial step, an amine-terminated hydrocarbon chain protected with a trifluoroacetamide functional group was attached to nanocrystalline diamond. The diamond surface was illuminated with UV light; this process led to activation of the diamond surface. Next, an electrophilic attack to the cross-linking double bond was carried out. The protected amine was subsequently deprotected, resulting in a primary amine. The amine was then reacted with a cross-linker molecule. The material was finally reacted with thiol-modified DNA. Hybridization reactions with fluorescently tagged oligonucleotides showed no detectable nonspecific adsorption. In addition, DNA-modified ultrananocrystalline diamond surfaces showed no measurable decrease in signal intensity after thirty cycles. It is believed that DNA-modified diamond surfaces are more resistant to oxidation than Si-O or thiol-gold interactions. More recently, Popov *et al.* showed ribonucleic acid molecule attachment to a nanocrystalline diamond/amorphous carbon composite; in this study, 1-amino-3-cyclopentene hydrochloride was attached to nanocrystalline diamond using UV irradiation[52]. Haertl *et al.* attached proteins, including catalase and green fluorescent protein, to nanocrystalline diamond using a covalent mechanism[53]. In the initial step, an amine-containing molecule was immobilized on hydrogen-terminated nanocrystalline diamond using a photochemical process; proteins were attached to the surface using peptide bonds. Catalase-modified nanocrystalline diamond electrodes were demonstrated for use as hydrogen peroxide sensors.

Rubio-Retama *et al.* demonstrated immobilization of an enzyme on nanocrystalline diamond[54]. In the initial step, TFA (2,2,2-trifluorine-N-9'-decenil acetamide) was attached to nanocrystalline diamond using a photochemical process. Enzyme attachment involved TFA attachment, TFA deprotection, insertion of a carboxyl group, and immobilization of the enzyme (horseradish peroxidase). The proximity of the horseradish peroxidase heme groups to the nanocrystalline diamond enabled direct electron transfer. This electrode was used to detect hydrogen peroxide in the 0.1 – 45 mM range; enzymatic activity for the biosensor was constant over fifteen days at room temperature. This system may be used in amperometric biosensors or enzyme-linked immunosorbent assays.

In addition, Zhou *et al.* have described covalent immobilization of cytochrome c on boron-doped nanocrystalline diamond[55]. A

photochemical reaction was used to chemically modify hydrogen-terminated nanocrystalline diamond surfaces with an undecylenic acid methyl ester. The ester was hydrolyzed under basic conditions to create a monolayer of carboxylic groups; cytochrome c was covalently immobilized on the carboxyl-terminated electrode by means of a carbodiimide coupling reaction. Direct electron transfer between cytochrome c and the electrode was observed. Response to a H_2O_2 concentration between 1 and 450 μM was observed; excellent electrocatalytic performance (e.g., low detection limit, rapid response, and high stability) was also noted.

Modification of diamond powders has been demonstrated. For example, Nguyen *et al.* described modification of diamond through a physical adsorption process[56]. Diamond powders (with a size of 100 nm) underwent treatment in oxidative acid solution (concentrated H_2SO_4 and HNO_3 mixture) at elevated temperatures. Noncovalent immobilization of the hen egg white lysozyme enzyme, an antimicrobial protein, was subsequently performed. The enzyme retained significant activity after physical adsorption to the crystallite surface. Co-adsorption of cytochrome c, a heme protein involved with electron transfer within the mitochondrial electron transport chain, on the crystallite surface served to block empty sites, enhance surface crowding, and increase enzyme activity.

Binding of biotin, a B-complex vitamin commonly utilized in *in vitro* biochemical assays, to diamond has also been demonstrated. Neugart *et al.* utilized a surfactant (sodium dodecyl sulfate) to improve stability of nanodiamond solutions and reduce nanodiamond aggregation[57]. After incubation, nanodiamond particles entered the cells within a few minutes. The 50 nm nanodiamond particles were shown to enter the cell via the endosomal pathway. Binding of streptavidin to biotinylated nanodiamond aggregates was also shown. Since each streptavidin molecule can bind four biotin molecules, large aggregates were formed.

The Fenton reaction has been used to create functionalized nanodiamond particles. Martin *et al.* exposed raw nanodiamond particles (of particle size 7 nm) to the Fenton reaction in order to remove amorphous soot, increase surface-OH groups, and enable covalent functionalization[58]. They functionalized nanodiamond with thionine; these nanoparticles were shown to enter HeLa cell nuclei. 97 % of HeLa cells survived after incubation with nanodiamond-thionine, indicating good biocompatibility.

In recent work, Sreenivasan *et al.* demonstrated salt-solution stable bioconjugation of luminescent nanodiamond particles with barstar:barnase, a high-affinity protein pair[30]. The covalent nature of the luminescent nanodiamond particle-barstar bonding was demonstrated using x-ray photoelectron spectroscopy. Luminescent nanodiamond-barstar conjugates in buffer solutions were noted to be stable over several months. Imaging of luminescent nanodiamond-barstar:barnase-enhanced green fluorescent protein particles within Chinese hamster ovary cells was also demonstrated.

Drug delivery using nanodiamond

Immobilization of chemotherapeutic agents on nanodiamond has been described. Huang *et al.* functionalized 2 – 8 nm nanodiamond particles with doxorubicin hydrochloride (DOX); doxorubicin hydrochloride is a pharmacologic agent that is used to induce apoptosis (controlled cell death)[59]. A detonation technique was used to produce nanodiamond material, which contained hydrophilic functional groups such as –COOH and -OH. Biocompatibility of nanodiamond was demonstrated using a real-time polymerase chain reaction. Genes associated with expression of interleukin-6, tumor necrosis factor α, and inducible nitric oxide synthase were not significantly up-regulated in cells exposed to nanocrystalline diamond, indicating the absence of inflammation.

Sodium chloride was shown to promote the adsorption of doxorubicin hydrochloride onto nanodiamond; 2 – 10 nm coatings were observed on the nanodiamond particles using transmission electron microscopy. Release of doxorubicin hydrochloride was obtained by removal of sodium chloride. Their work showed that doxorubicin-nanodiamond composites induced cell death in murine macrophage and HT-29 colorectal cancer cells. Furthermore, MTT assays and DNA fragmentation assays revealed that doxorubicin-nanodiamond composites were associated with apoptotic cell death.

Covalent immobilization of paclitaxel on nanodiamond was demonstrated by Liu *et al.*[60]. Nanodiamond-paclitaxel (of concentration 0.1 – 50 μg ml^{-1}) inhibited mitosis and induced apoptosis in A549 human lung cells. Confocal microscopy indicated that the 3 – 5 nm nanodiamond particles were localized in the cytoplasm and in the microtubules. Nanodiamond-paclitaxel particles were shown to block tumor growth and lung cancer cell formation in xenograft SCID mice. In this study, nanodiamond particles and paclitaxel were joined by an ester bond, which can be broken by esterase enzymes. Nanodiamond particles alone induced neither apoptosis nor mitotic arrest. In addition, delivery of water-insoluble pharmacologic agents has been demonstrated. Chen *et al.* used an acid treatment to remove impurities and form carboxyl groups on the surfaces of nanodiamond particles[61]. The carboxyl groups enabled the nanodiamond suspension to be stable in water. The carboxyl groups were also capable of complexing with poorly water-soluble drugs; for example, attachment of three drugs, purvalanol A (a drug for liver cancer), 4-hydroxytamoxifen (a drug for estrogen receptor-positive breast cancer), and dexamethasone (an anti-inflammatory agent), was demonstrated.

Zhang *et al.* demonstrated plasmid DNA delivery using nanodiamond[62]. They immobilized 800 Da polyethyleneimine, a polycation used for transfection, on the surface of nanodiamond. This material demonstrated high transfection efficiency in a HeLa cell model, which was similar to that of high molecular weight polyethyleneimine (25K). 80 % of cells survived in the medium containing polyethyleneimine 800-nanodiamond at concentrations as high as 90 μg/mL. A combination of 800 Da polyethyleneimine and nanodiamond was noted to provide the high transfection efficiency of

high molecular weight polyethyleneimine and the low cytotoxicity of low molecular weight polyethyleneimine. The combination of 800 Da polyethyleneimine and nanodiamond may also include other medically-relevant agents, such as chemotherapeutic agents and cell-specific targeting molecules.

Chow *et al.* recently utilized a complex containing nanodiamond and doxorubicin for treatment of mammary carcinoma and hepatoblastoma (liver tumor) in a murine model[63]. *In vivo* studies showed that intravenous delivery of nanodiamond-doxorubicin complexes provided increased retention within tumor cells and greater inhibition of tumor growth than intravenous delivery of doxorubicin; no increases in systemic immune response (as indicated by serum interleukin-6), liver toxicity (as indicated by serum alanine transferase), or myelosuppression were associated with nanocrystalline diamond treatment. Although retention of nanodiamond-doxorubicin complexes was enhanced in both tumor tissues and healthy tissues, clearance of the small nanodiamond-doxorubicin complexes from slowly dividing healthy tissue cells prevented systemic apoptosis (programmed cell death) in healthy tissues. Their work suggests that nanodiamond-based chemotherapeutic agents may be useful for treatment of tumors that are resistant to conventional chemotherapeutic agents.

Imaging with nanodiamond:

Several studies have demonstrated imaging of nanodiamond particles within cells and tissues[64]. As noted by Barnard, the fluorescence properties of diamond are associated with point defects, including nitrogen-vacancy and silicon-vacancy defects[28]. Nitrogen-vacancy defects are of particular interest for imaging applications because they exhibit strong absorbance at 560 nm and fluorescence at approximately 700 nm[64]. For example, Yu *et al.* created point defects in diamond, specifically negatively charged nitrogen vacancy center (N-V)- defects, by means of a two-step process that involved (a) irradiation-induced damage using a 3 MeV proton beam and (b) thermal annealing at 800 °C for 2 hours under vacuum[65]. Synthetic type Ib diamond powders with a nominal size of 100 nm were prepared by irradiation-annealing; these particles exhibited a 10^2-fold enhancement in fluorescence intensity compared with annealed materials. The fluorescent nanodiamond materials were shown to be suitable for epifluorescent imaging. Entry of fluorescent nanodiamond particles to the cell and localization within the cytoplasm was demonstrated. In addition, an MTT assay involving 293T human kidney cells revealed an absence of toxicity.

Chang *et al.* prepared magnetic nanodiamond particles from a mixture of annealed nanodiamond powder and ferrocene powder by means of microwave irradiation-induced arcing; nanodiamond particles with a coercivity field of 155 G and a saturation magnetization of ~10 emu/g were obtained using this approach[66]. Magnetic nanodiamond particles with fluorescent properties were created by grafting fluorescein o-methacrylate onto magnetic nanodiamond particles using microwave irradiation. Ingestion of fluorescent magnetic nanodiamond particles into the cytoplasms of HeLa cells via nonreceptor-mediated endocytosis was demonstrated.

Fu *et al.* described bright fluorescence from diamonds at 550 – 800 nm[67]. Fluorescence of a single 35 nm diamond was noted to be significantly brighter than that of a single Alexa Fluor 546 dye molecule under the same excitation conditions. The nanodiamond particles showed no sign of photobleaching even after 5 minutes of continuous excitation by 532 nm light at a power density of 8×10^3 W/cm^2. 35 nm fluorescent nanocrystalline diamond particles were incubated with HeLa cells. Vertical cross-section images demonstrated translocation of the fluorescent nanocrystalline diamond particles through the cell membrane. Many fluorescent nanocrystalline diamond particles formed aggregates in the cell. The particles exhibited photostability after continuous excitation for 20 minutes (with a laser power of 100 W/cm^2). Neither photobleaching nor blinking of fluorescence was noted. In addition, tracking of a 35 nm single fluorescent nanocrystalline diamond particle in the cytoplasm of a live HeLa cell was demonstrated.

Nanodiamond has recently been considered for use as a biomarker. For example, Chang *et al.* created bright fluorescent nanodiamonds in large quantities through formation of point defects in synthetic diamond nanocrystallites by means of 40 keV He^+ helium ion irradiation from a radio-frequency ion source[68]. Excellent photostability was observed in the modified 25 nm nanoparticles. Imaging and three-dimensional tracking of fluorescent nanodiamond in a HeLa cell using two-photon excitation microscopy was demonstrated. Biodistribution of nanodiamond has been examined by means of radiolabeling. For example, Yuan *et al.* used radiolabeling, Raman spectrometry, transmission electron microscopy, and UV-visible light spectroscopy to examine biodistribution of iodine 215-labeled ~50 nm nanoparticles in a male ICR murine model[69]. Fig. 6 shows high-resolution transmission electron microscopy images of digested solutions containing murine liver, lung, and spleen tissues twenty eight days after nanodiamond particle injection. 60 % of nanodiamond particles were observed in the liver at thirty minutes. It is believed that nanocrystalline diamond particles are rapidly captured by opsonization; the nanoparticles are bound by opsonins in the plasma and are subsequently recognized by phagocytes in the reticuloendothelial system.

Zhang *et al.* prepared radiolabeled nanodiamond particles and examined the biodistribution of these particles after intratracheal instillation in a Kun Ming mouse model[70]. They showed that a majority of the intratracheally administered ^{188}Re-nanodiamond particles remained in the lungs; however, some particles crossed the blood-air barrier and entered the bone, heart, liver, and spleen. They also observed dose-dependent systemic toxicity involving several tissues; for example, dose-dependent adverse effects on kidney and lung function were observed. Faklaris *et al.* examined the use of photoluminescent nanodiamond (of size 50 nm) as a biomarker in

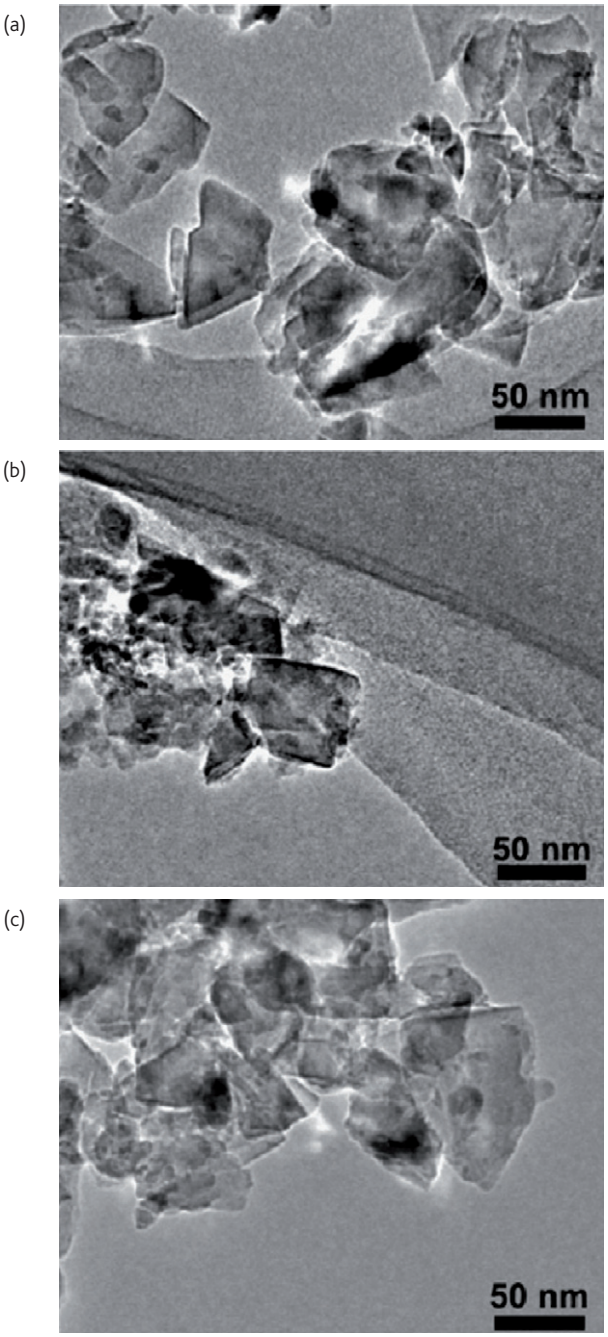

Fig. 6 High-resolution transmission electron microscopy images of digested solution of different mouse tissues at 28days after intravenous injection of 80mg/kg body weight nanodiamonds. (a) Liver, (b) spleen, and (c) lung. Reprinted from[70] with permission from Elsevier.

diagnostic and therapeutic applications[71]. They attributed emission in the red and near-infrared spectral region (575 – 750 nm) to nitrogen vacancy color centers. In addition, they noted that photoluminescent nanodiamond materials did not exhibit photobleaching or photoblinking. Photoluminescent nanodiamond was shown to enter cells by means of endocytosis; it is believed that this process is mediated by clathrin. Once in the cells, nanodiamond particles were segregated in endosomal and lysosomal vesicles; some of these materials were released into the cytoplasm. *In vitro* studies involving HeLa cells demonstrated an absence of cytotoxicity. These photoluminescent nanodiamond materials may be used for imaging transport and labeling intracellular structures.

The use of labeled nanodiamond has clinical applications; for example, nanodiamond particles containing gadolinium (III) have been considered for use in magnetic resonance imaging (MRI). Manus *et al.* described the use of gadolinium (III)-nanodiamond particles in MRI[72]. An amine-functionalized Gd(III) complex with a six carbon linker was reacted with carboxylic acid groups on the surface of nanodiamond. The hydrodynamic size of gadolinium (III)-nanodiamond decreased from ~128 to ~55 nm after dilution and ultrasonication; the pre-conjugation size of the nanodiamond was ~21 nm. Gadolinium (III)-nanodiamond did not significantly decrease cell viability compared to doxorubicin. In addition, gadolinium (III)-nanodiamond had no significant effect on cytotoxicity in comparison with unmodified nanodiamonds in HeLa cells or unmodified nanodiamonds in NIH/3T3 cells below a concentration of 0.5 mg mL^{-1}. They demonstrated improved performance, including ten-fold greater relaxivity values as well as significantly higher contrast levels, with gadolinium-modified nanodiamond in comparison with conventional Gd(III) complex.

As discussed by Barnard, coherent interfacial Coulombic interactions result in agglomeration of as-prepared nanodiamond particles[28]. Recent work has indicated that functionalization with polyethylene glycol may be used to prevent nanodiamond aggregation. For example, Takimoto *et al.* recently incorporated polyethylene glycol and fluorescein on the surface of diamond[73]. In the initial step, ω-aminododecanoic acid was immobilized on the surface of nanodiamond particles. These fluorescent nanoparticles remained in dispersion within a phosphate-buffered saline physiological solution. In addition, use of the functionalized nanodiamond particles for cellular imaging in HeLa cells was demonstrated.

It should also be noted that Raman spectroscopy may be utilized as a noninvasive contrasting approach with nanodiamond particles[29]. The Raman spectra of materials containing sp^3-hybridized carbon bonds show a strong intensity signal at 1332 cm^{-1}, which is associated with a triply-degenerate zone center optical phonon exhibiting F_{2g} symmetry[74,75]. For example, Cheng *et al.* utilized confocal Raman mapping to perform *in vitro* monitoring of interactions between carboxylated nanodiamond-growth hormone complexes and growth hormone receptors in A549 human epithelial cells[76].

Summary

The results of recent studies have demonstrated the use of diamond in a variety of medical applications, including drug delivery devices, microelectromechanical devices, and cardiovascular devices. However, several challenges for diamond-based materials and devices must be overcome. Reproducible, scalable processes must be developed to

facilitate the translation of diamond coatings to clinical use. The short-term toxicity, long-term toxicity, and fate of diamond, impurities, and breakdown products must be carefully considered using medical application-specific parameters[26,77]. Additional work is also necessary to optimize the properties of diamond for particular medical applications. Efforts are underway to increase the density of nitrogen-vacancy point defects in small (< 5 nm) nanodiamond particles; for example, Smith *et al.* prepared nanodiamond particles containing nitrogen-vacancy point defects by means of high-energy (2.5 MeV) proton irradiation and thermal annealing[28,78]. The relationships between biological functionality, surface functionalization, purity, and physical properties (e.g., aspect ratio) must also be carefully considered[29]. Furthermore, improved methods for conjugating pharmacologic agents and biological molecules to diamond must be developed[29]. If these hurdles are overcome, diamond-based materials and devices may be translated to use in medical devices, drug delivery, and medical diagnostic applications over the next few decades. mt

Acknowledgments:

One of the authors (AVS) would like to acknowledge use of the Center for Nanoscale Materials, which is supported by the U. S. Department of Energy, Office of Science, Office of Basic Energy Sciences, under Contract No. DE-AC02-06CH11357.

REFERENCES

1. Narayan, R J., and Boehm, R., Hard as Diamonds, *Med Device Develop* (2010) **2**.
2. Ramachandran, G. N., *Nature* (1945) **156**, 83.
3. Pierson, H., Handbook of carbon, graphite, and fullerenes: properties, processing, and applications, Noyes Publications, Park Ridge, NJ (1993).
4. Bundy, F. P., *et al.*, *Nature* (1955) **176**, 51.
5. Eversole, E. G., Synthesis of Diamond. Patent number 3,030,187, 1962.
6. Derjaguin, B. V., and Fedoseev, D. B., *Sci Am* (1975) **233**, 102.
7. Angus, J. C., *et al.*, *J Appl Phys* (1968) **39**, 2915.
8. Anthony, T. R., *Vacuum* (1990) **41**, 1356.
9. Zhou, D., *et al.*, *J Appl Phys* (1998) **84**, 1981.
10. Kumar, A., *et al.*, *Thin Solid Films* (1997) **308**, 209.
11. Williams, O. A., *et al.*, *Chem Phys Lett*(2007) **445**, 255.
12. Kromka, A., *et al.*, *Chem Vapor Depos* (2008) **14**, 181.
13. Godbole, V. P., *et al.*, *Mater Sci Eng B* (1999) **58**, 251.
14. Belmonte, M., *et al.*, *Diam Relat Mater* (2003) **12**, 733.
15. Mallika, K., *et al.*, *Thin Solid Films* (2001) **396**, 146.
16. Butler, J. E., and Sumant, A. V., *Chem Vapor Depos* (2008) **14**, 145.
17. Amaral, M., *et al.*, *Surf Coat Technol* (2010) **204**, 1962.
18. Gruen, D. M., *MRS Bullet* (2001) **26**, 771.
19. Jiao, S., *et al.*, *J Appl Phys* (2001) **90**, 118.
20. Sumant, A. V., *et al.*, *SPIE Proceedings: Micro- and Nanotechnology Sensors, Systems, and Applications* (2009) **7318**, 71817.
21. Naguib, N. N., *et al.*, *Chem Phys Lett* (2006) **430**, 345.
22. Sumant, A. V., *et al.*, *MRS Bullet* (2010) **35**, 281.
23. Sumant, A. V., *et al.*, *Phys Rev B* (2007) **76**, 235429.
24. Narayan, R.J., *et al.*, *Diam Relat Mater* (2006) **15**, 1935.
25. Adadurov, G. A., *et al.*, Methods of producing diamond and/or diamond-like modifications of boron nitride. United States Patent 4,483,836, 1984.
26. Schrand A. M., *et al.*, *CRC Cr Rev Sol State* (2009) **34**, 18.
27. Krueger, A., *et al.*, *Carbon* (2005) **43**, 1722.
28. Barnard, A. S., *Analyst* (2009) **134**, 1751.
29. Lam, R., and Ho, D., *Expert Opin Drug Del* (2009) **6**, 883.
30. Sreenivasan, V. K., *et al.*, *J Mater Chem* (2001) **21**, 65.
31. Fries, M. D., *et al.*, *J Phys D* (2002) **35**, L105.
32. Papo, M. J., *et al.*, *J Mater Sci: Mater M* (2004) **15**, 773.
33. Jozwik, K., *et al.*, *Diam Relat Mater* (2007) **16**, 1004.
34. Amaral, M, *et al.*, *Diam Relat Mater* (2007) **16**, 790.
35. Pecheva, E., *et al.*, *Surf Interface Anal* (2010) **42**, 475.
36. Huang, H., *et al.*, *ACS Nano* (2008) **2**, 203.
37. Sumant, A. V., *et al.*, *Adv Mater* (2005) **17**, 1039.
38. Hamilton, M. A., *et al.*, *Proceedings of the STLE/ASME International Joint Tribology Conference* (2008) IJTC2008-71198.
39. Krauss A. R., *et al.*, *Diam Relat Mater* (2001) **10**, 1952.
40. Auciello, O., *et al.*, *J Phys – Condens Matt* (2004) **16**, R539.
41. Khanna. P., *et al.*, *Diam Relat Mater* (2006) **15**, 2073.
42. Khanna. P., *et al.*, *Diam Relat Mater* (2009) **18**, 606.
43. Bijnens, N., *et al.*, *Physica Status Solidi A* (2008) **205**, 520.
44. Nebel, C. E., *et al.*, *Diam Relat Mater* (2009) **18**, 910.
45. Ariano, P. *et al.*, *Eur J Phys E* (2009) **30**, 149.
46. Ariano, P., *et al. Biosens Bioelectron* (2009) **24**, 2046.
47. Dankerl, M., *et al.*, *Adv Funct Mater* (2009) **19**, 2915.
48. Xiao, X. C., *et al.*, *J Biomed Mater Res* (2006) **77B**, 273.
49. Bonnauron, M., *et al.*, *Phys Stat Sol A* (2008) **9**, 2126.
50. Rezek, B., *et al.*, *Biosens Bioelectron* (2010) **26**, 1307.
51. Yang, W. S., *et al.*, *Nature Mater* (2002) **1**, 253.
52. Popov, C., *et al.*, *Diam Relat Mater* (2008) **17**, 882.
53. Haertl, A., *et al.*, *Nature Mater* (2004) **3**, 736.
54. Rubio-Retama, J., *et al.*, *Langmuir* (2006) **22**, 5837.
55. Zhou, Y., *et al.*, *Anal Chem* (2008) **80**, 4141.
56. Nguyen, T. T. B., *et al.*, *Diam Relat Mater* (2007) **16**, 872.
57. Neugart, F., *et al.*, *Nano Letters* (2007) **7**, 3588.
58. Martin, R., *et al.*, *ACS Nano* (2010) **4**, 65.
59. Huang, H., *et al.*, *Nano Letters* (2007) **7**, 3305.
60. Liu, K. K., *et al.*, *Nanotechnology* (2010) **21**, 315106.
61. Chen, M., *et al.*, *ACS Nano* (2009) **3**, 2016.
62. Zhang, X. Q., *et al.*, *ACS Nano* (2009) **3**, 2609.
63. Chow, E. K., *et al.*, *Science Translational Medicine* (2011) **3**, 73ra21.
64. Hui, Y. Y., *et al.*, *J Phys D* (2010) **43**, 374021.
65. Yu, S. J., *et al.*, *J Am Chem Soc* (2005) **127**, 17604.
66. Chang, I. P., *et al.*, *J Am Chem Soc* (2008) **130**, 15476.
67. Fu, C. C., *et al.*, *PNAS USA* (2008) **104**, 727.
68. Chang, Y. R., *et al.*, *Nature Nanotechnol* (2008) **3**, 284.
69. Yuan, Y., *et al.*, *Diam Relat Mater* (2009) **18**, 95.
70. Zhang, X., *et al.*, *Toxicol Lett* (2010) **198**, 237.
71. Faklaris, O., *et al.*, *ACS Nano* (2009) **3**, 3955.
72. Manus, L. M., *et al.*, *Nano Letters* (2009) **10**, 484.
73. Takimoto, T., *et al.*, *Chem Mater* (2010) **22**, 3462.
74. Schiferl, D., *et al.*, *J Appl Phys* (1997) **82**, 3256.
75. Levenson, M. D., *et al.*, *Phys Rev B* (1972) **6**, 3962.
76. Cheng, C. Y., *et al.*, *Appl Phys Lett* (2007) **90**, 163903.
77. Krueger, A., *Chem - Eur J* (2008) **14**, 1382.
78. Smith, B. R., *et al.*, *Small* (2009) **5**, 1649.